Polymer 55 (2014) 6091–6101

Contents lists available at ScienceDirect

Polymer

journal homepage: www.elsevier.com/locate/polymer

Mapping micromechanical properties of soft polymer contact lenses

Marius Chyasnavichyus, Seth L. Young, Vladimir V. Tsukruk*

School of Materials Science and Engineering, Georgia Institute of Technology, Atlanta, GA 30332, United States

ARTICLE INFO

Article history:
Received 30 June 2014
Received in revised form
17 September 2014
Accepted 21 September 2014
Available online 28 September 2014

Keywords:
Micromechanical properties
Soft contact lenses
AFM measurements

ABSTRACT

We present comparative micromechanical characterization of several commercial soft silicone hydrogel contact lenses, which allows for the examination of spatial distribution of different regions with local mechanical properties within the lens under practical wet conditions. We employ elastic contact mechanic model and corresponding analysis of force–distance curves collected with high-resolution atomic force microscopy measurements performed within elastic deformation limits. The measurements were performed on the lens cross section to map the micromechanical properties distribution within the subsurface regions and bulk material of the different lens. In addition, we have studied topography and mechanical properties of the lens surfaces, which come into direct contact with the surface of the eye and eyelid. AFM images show high contrast distribution maps for the adhesive and mechanical properties of the different microstructured regions such as pores, lamellae and different material inclusions within the lenses. Additional indentation experiments allow for collection of quantitative data for micromechanical properties from different regions within the lens structure and correlate these data with lens-averaged macroscopic measurements available in the literature.

1. Introduction

The mechanical properties of silicone hydrogel contact lenses, which critically depend upon lens water content, porosity, and oxygen permittivity, are the most important parameters affecting their ultimate performance [1]. State of the art contact lens materials should be soft and flexible enough to provide comfort to the wearer and reduce complications associated with constant stress within the eye such as papillary conjunctivitis and changes in corneal curvature [2,3]. At the same time the lens material needs to be rigid enough to maintain overall shape and withstand multiple stress cycles in saline environments, while prolonging optical performance and clarity during extended wear [4].

The introduction of silicone hydrogel materials for lens fabrication has allowed for the design of new, high performance lenses. Because these silicone-based materials are intrinsically hydrophobic and have higher elastic moduli than previous generations of lens materials, much focus has been placed on increasing water content and oxygen transport in the lens and reducing surface stiffness for maximum comfort to the wearer [5–7]. For example, to reduce differences in surface chemistry between the lens material and the ocular surface while preventing tear film breakup, a surface coating can be applied or wetting agents can be incorporated into the bulk of the lens structure. Most popular current designs involve physical and chemical surface treatments to address these issues and modify lens–eye interactions including adhesion and lubrication [8]. Therefore, it becomes even more important to precisely characterize local mechanical properties distributions of these multiphase materials under relevant practical conditions in addition to traditional tensile testing.

Most current mechanical measurement methods involve conventional tensile testing to evaluate elastic modulus of the lens materials [9,10]. However these conventional tensile methods have several drawbacks. First, it is hard to compare the stiffness of different contact lenses as the measurements strongly depend on the sample preparation: such factors as small defects introduced during fabrication or clamping prior to testing and differences in thickness between lenses with different optical power dramatically reduce the precision. Second, the complex near semi-spherical sample shape makes measured values vary greatly; thus a simple flat slab shape is frequently used instead of actual lenses for tensile testing [11]. Furthermore, tensile tests are only able to provide an averaged elastic modulus of the entire lens, without any means to differentiate specific local properties from the lens components. In the case of surface modification of contact lenses the mechanical properties of the coating will dominate in the eye-lens contact interface although the overall rigidity is controlled by the bulk properties of lens matrices [12]. Thus high resolution, spatially

* Corresponding author.
E-mail address: vladimir@mse.gatech.edu (V.V. Tsukruk).

http://dx.doi.org/10.1016/j.polymer.2014.09.053
0032-3861/

capable techniques should be employed to evaluate distributed mechanical properties of multiphase lens materials.

The AFM-based surface force spectroscopy (SFS) technique is a well known approach for the characterization of micromechanical properties of multiphase polymeric materials with nanoscale resolution [13,14]. This technique was successfully used for micromechanical characterization of complex polymeric composite materials, grafted polymers, natural polymers, nanoscale polymer films, soft biomaterials and individual molecules [15–27]. AFM-based techniques have been widely used in vision science to study surface topography [28], friction [29], and protein absorption [30] for contact lens materials and eye tissue [17,31], however they are rarely used for probing surface mechanical properties of this class of materials due to the complexity of probing under wet conditions.

Several successful examples of measuring micromechanical properties of the surface layers of hydrogel contact lens have been published by Somorjai et al. [32,33]. In these studies, it was found that elastic modulus of the lens surface depends strongly on the loading rate and water content within the lens. However only thin surface regions were studied and the spatial distribution of mechanical properties across the lens surface and sub-surface regions was not examined in this study. To the best of our knowledge, no studies on the variations in mechanical properties of different structural regions within the soft contact lenses (exterior and interior) have been performed to date.

From an experimental prospective, such measurements can be performed in two probing manners: the fast, high-frequency force-tapping mode (under different common trade names such as Bruker's Quantitative Nanomechanics (QNM)) and by using standard surface force spectroscopy (SFS) in which a two dimensional array of force–distance curves (FDCs) is collected in static mode and analyzed [34]. FDCs collected in both ways contain tip sample interaction information and can be used to calculate sample mechanical properties using known tip parameters and different models of contact mechanics [35,36]. In the force-tapping mode, an AFM tip is driven sinusoidally at frequencies much lower than the cantilever's first resonant peak (typically 1 or 2 kHz) and briefly interacts with the sample surface in the middle of each cycle [37]. This measurement mode allows for the determination of various mechanical properties of the sample surface, such as elastic modulus and adhesion, as well as surface topography with high resolution in a short amount of time. However, as a result of the short interaction time, the mechanical measurements performed in this mode lack precision and usually only provide qualitative contrast maps of surface distribution of mechanical properties [14]. In SFS, the AFM tip moves in saw tooth-like motion indenting into the sample during each cycle. Due to the piezoelement mobility limitations, the frequency of these indentations are limited to several tens of Hz [38], however the well-defined FDCs enables the determination of quantitative data for the material with high precision [13].

In present study we suggest a practically-valuable methodology to characterize spatial distribution of mechanical properties within the soft microstructured materials of commercial contact lenses including both exterior and interior microscopic regions. Using commercially-available soft silicone hydrogel contact lens materials as an example we demonstrate that high frequency measurements to acquire high resolution maps of topography and mechanical properties can be combined with static FV nano-indentations to provide reliable micromechanical measurements to such complex composite materials under wet conditions. We mapped the micromechanical properties of the lens surface as well as lens cross-sections to reveal complex sub-surface morphology with greatly different elastic responses that cannot be obtained with conventional macroscopic mechanical testing.

2. Experimental

2.1. Contact lens preparation

In this work, four different commercially available silicone-hydrogel contact lens brands were selected for comparative studies: Balafilcon A (Purevision, Bausch & Lomb Inc.), Senofilcon A, (Acuvue Oasis, Johnson & Johnson Vision Care Inc.), Lotrafilcon B (AirOptix Aqua, CIBA Vision Corp.) and Comfilcon A (Biofinity, CooperVision Inc.) purchased through Contactlenses Ltd. Manufacturer reported values for several physical characteristics of these lenses are summarized in Table 1.

Lenses were measured immediately after removal from their original blister pack and discarded after one day of measurements. Each lens was sectioned into several pieces using steel razor blades under wet conditions to avoid any drying (Scheme 1, a). The lenses were attached to metal sample disks (Ted Pella Inc.) using double sided tape for AFM measurements on the lens surface (Scheme 1, b). The measurements were performed within a small droplet of saline solution (taken from the blister pack) covering the piece of the lens deposited onto the metal disc. For AFM measurements of the lens cross-sections, pieces of the lens were firmly locked between two metal plates with the freshly cut surface facing upwards (Scheme 1, c). Both metal plates were fully submerged in the liquid for the measurement. To find regions suitable for the AFM measurements, lens sections were examined with a high resolution microscope (BX51, Olympus) in the dry state followed by quick rehydration. Poly(dimethyl siloxane) (PDMS) was used as a control model substrate for elastic modulus measurements [39]. Centimeter-thick PDMS substrates were prepared using a Sylgard 184 Silicone Elastomer Kit (Dow Corning, USA). The elastomer base was vigorously mixed with curing agent in a 5:1 ratio (w:w) for 10 min, then placed under vacuum at room temperature for 30 min in order to remove all remaining air bubbles. The mixture was cured overnight at 70 °C and allowed to cool before use in AFM measurements.

2.2. AFM measurements

AFM and SFS measurements were performed with a Dimension Icon AFM microscope (Bruker). All measurements were performed with the lens submerged in the original solution from the lens package using a fluid cell. Soft aluminum coated AFM tips (Mikromasch) with nominal spring constants of 0.2 N/m were used for the measurements. Prior to each new sample measurement full tip characterization was conducted. Tip shape was estimated using the blind estimation method using a titanium roughness sample (Bruker) (see Fig. S1, Supporting Information). The blind estimation method allows for precise imaging of the AFM tip by scanning surfaces with sharp features [40]. The observed radius of curvature of the tips varied within the 10–30 nm range. Deflection sensitivity was determined by making FDCs on a sapphire crystal and the spring constant was calculated using the thermal calibration method.

Table 1
The characteristics of contact lenses used in this study.

Name	Manufacturer	Material	Water content[a], %	Surface treatment	Modulus, MPa[a]
Air Optix	Ciba Vision	Lotrafilcon B	33	Plasma coating	1.0
PureVision	Bausch and Lomb	Balafilcon A	36	Plasma oxidation	1.1
Acuvue Oasys	Johnson and Johnson	Senofilcon A	38	NA	0.72
Biofinity	CooperVision	Comfilcon A	48	NA	0.75

[a] Manufacturer reported values from Ref. [7].

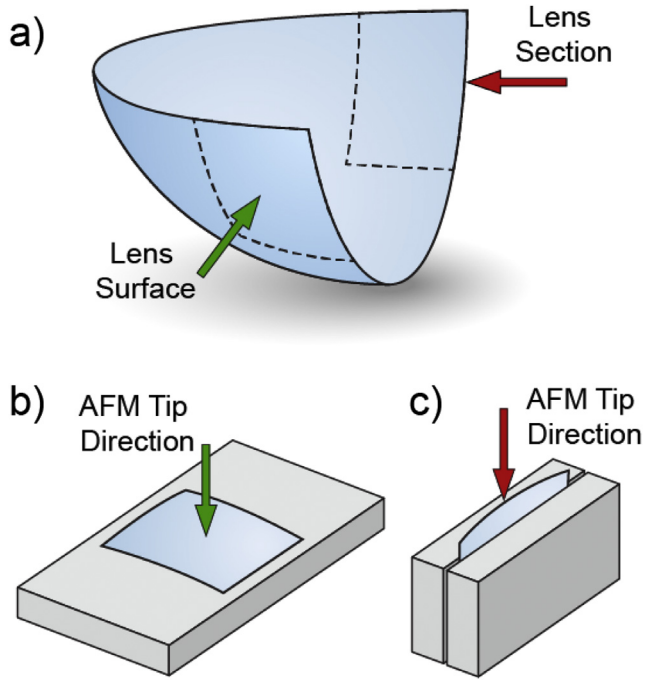

Scheme 1. Schematic of the lens preparation and mounting: a) Lens sectioning, b) Flat mounting for surface measurements, c) Side mounting for cross-section measurements. Red and green arrows show AFM tip direction during scan for flat cross-section and surface. (For interpretation of the references to color in this legend, the reader is referred to the web version of this article.)

High resolution (1024 × 1024 pixels) images were acquired in QNM mode at 1 kHz tip vibration frequency. In addition to surface topography, these measurements provide simultaneous contrast variation for regions with differences in stiffness and adhesive properties [41]. From the topographic images root mean squared (rms) microroughness values were calculated for randomly selected 1 × 1 μm^2 and 10 × 10 μm^2 surface areas. Of all three channels only the topography channel presents quantitative data; DMT modulus channel and adhesion channel show qualitative contrast images and z-scale for these measurements were not scaled to show real physical quantities. For the actual quantitative mechanical measurements FDCs were collected from the selected regions of the lens surface. All curves for mapping were collected at 4 Hz frequency (with 0.25 s per approach-retract indentation cycle) with applied forces in the 3–12 nN range. For frequency variation experiments, the frequency was varied in 0.01–10 Hz range.

2.3. FDC analysis

FDC data was analyzed using Sneddon's model for a rigid axisymmetric punch [42] as described in detail elsewhere [43]. Briefly, tip deflection, d was measured as the tip was displaced by distance z towards the sample (Fig. 1a). After the tip-sample contact, the cantilever penetrates into the surface by the distance $\delta = z - d$. The force F exerted onto the tip during indentation can be calculated from the cantilever deflection as $F = kd$, where k is the spring constant of the tip. According to this model, this force can be related to the penetration assuming the elastic material behavior. The following equation is used for an axisymmetric tip with a parabolic cross-section (Fig. 1b) [41]:

$$F = \frac{4}{3}\sqrt{R}\,E'\,\delta^{3/2} \quad (1)$$

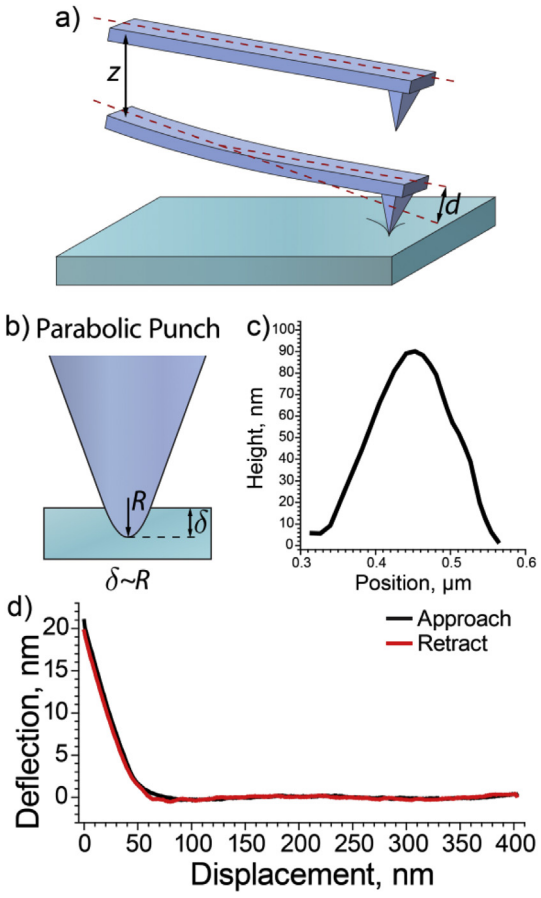

Fig. 1. a) AFM cantilever motion during indentation experiment. b) The AFM tip surface penetration for parabolic punch. c) Tip profile from tip shape reconstruction. d) Example of approach and retract curves for typical indentation experiment (bulk indentation into Comficon A).

where R is the radius of curvature of the apex of paraboloid, determined from the parabolic fitting of the reconstructed tip profile, and $E' = E/(1 - \upsilon^2)$ is the reduced modulus of the material with Poisson's ratio, υ, and Young's modulus, E, of the material. Poisson's ratio $\upsilon = 0.5$ was used in the present study under the usual assumption of incompressible elastic behavior of the lens materials. Curvature of the apex of the tip was calculated by fitting the tip shape (Fig. 1c) with the parabolic function.

Fitting of the $\delta^{3/2}$ penetration data versus force data with Eq. (1) allows for the calculation of the elastic modulus of the material. It is important to note that Sneddon's analysis cannot be performed in the presence of substantial adhesion between the surface and the tip [35]. However, in all cases in the present study, the adhesive force was at least 20 times lower than the maximum tip deflection, allowing for the assumption of zero adhesion (see an example in Fig. 1d). At least 36 force–distance curves were collected for each investigated region. For each curve the elastic modulus value was calculated and the mean value was determined from the set of the curves. All values are reported in this study as mean ± one standard deviation.

3. Results and discussion

3.1. AFM tip selection

For this high-resolution study, sharp 10–30 nm AFM tips were preferred to colloidal probes as a result of two governing factors.

First, the nanoscale lateral resolution attainable with small probes enables differentiation between various contact lens components. Second, sharper tips are advantageous for targeting specific regions of the sample with low roughness and tilt. Since Sneddon's model describes the interaction of a rigid punch with an elastic half space, only indentations into the flat regions of the sample are accurately described by the model.

In addition, colloidal and blunt probes are much less sensitive than sharper tips for the study of microscopic layered structures in which the layer thickness is much smaller than the size of the probe [44]. It is important to note, that colloidal probes have an advantage over sharp tips for measurements of the structural rigidity of composite materials [45] and in polymer brush studies [46].

3.2. Surface topography and mechanical properties

For this study the outer (convex) surface of the contact lens was chosen for the topography examination. Fig. 2 shows general topography of the lens surface. Topography images clearly show residual structural lines for all lens materials except Comfilcon A. These lines are usually attributed to mold defects, which are transferred to the lens surface during cast molding [47]. Despite the fact that all four lens types were manufactured by cast molding, Comfilcon A material does not show a characteristic web-like structure of linear defects. Instead, the surface of Comfilcon A lens is covered by a series of fine lines with less than 6 nm elevation. In addition to these features, the surface of Balafilcon A (Fig. 2b) shows deeper grooves which are likely small fractures of the outer layer appearing due to the plasma oxidation process [12], as well as elongated surface depressions about 60 nm deep. The roughness values within 2–20 nm are characteristic of very smooth surfaces and are close to those reported in literature for similar lenses [48,49]. For some lenses, such as Balafilcon A and Lotrafilcon B, at larger scale size (10 μm^2) (Table 2) the roughness is higher but at smaller scale (1 μm^2) all lenses show similar low roughness, therefore, in the indentation experiments these surfaces were considered to be flat.

Table 2
Surface microroughness values of the lens surfaces.

Material	Roughness 10 × 10 μm, nm	Roughness 1 × 1 μm, nm
Lotrafilcon B	7.1 ± 1.6	2.1 ± 0.4
Balafilcon A	15.8 ± 2.0	3.2 ± 0.4
Senofilcon A	3.2 ± 0.3	1.9 ± 0.3
Comfilcon A	2.4 ± 0.1	2.0 ± 0.1

All indentation experiments were performed in the flat regions between the linear grooves away of any surface irregularities. Typical FDCs in terms of tip deflection vs. displacement for the surface indentation experiments are presented in Fig. 3. Elastic moduli for the surfaces of all lens materials were calculated according to Eq. (1) by fitting $\delta^{3/2}$ versus force data with Sneddon's model. Results are summarized in Table 3.

By plotting the indentation data for Lotrafilcon A and Balafilicon A lenses as $\delta^{3/2}$ versus applied force (Fig. 4a and Fig. 4b, respectively), one can see two distinct linear regions, with the first region having higher slope than the second. Such behavior is characteristic for indentations into the soft thin film supported by stiffer substrate [50]. Indeed, as known, Lotrafilcon B and Balafilcon A lens materials are inherently hydrophobic [8], thus to provide wettability to the lens surface both materials are plasma treated. In the case of Lotrafilcon B, plasma polymerization results in a ~25 nm hydrophilic layer on the lens surface. For Balafilcon A plasma oxidation provides hydrophilic groups to the lens surface [51].

We suggest that the presence of these plasma treated surface layers is reflected in penetration data. In the case of Lotrafilcon B lens slope starts to change at ~28 nm penetration, which is close to thickness of the reported value of outer polymer layer [49].

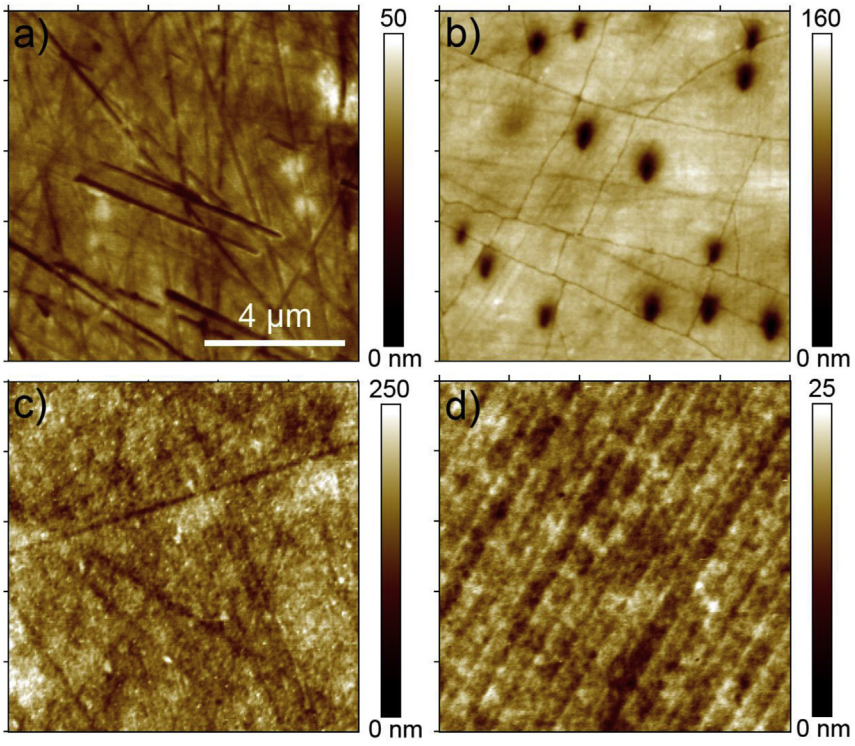

Fig. 2. Surface topography of submerged soft contact lenses used in this study. a) Lotrafilcon B, b) Balafilcon A, c) Senofilcon A, d) Comfilcon A. Scale bar is the same for all images.

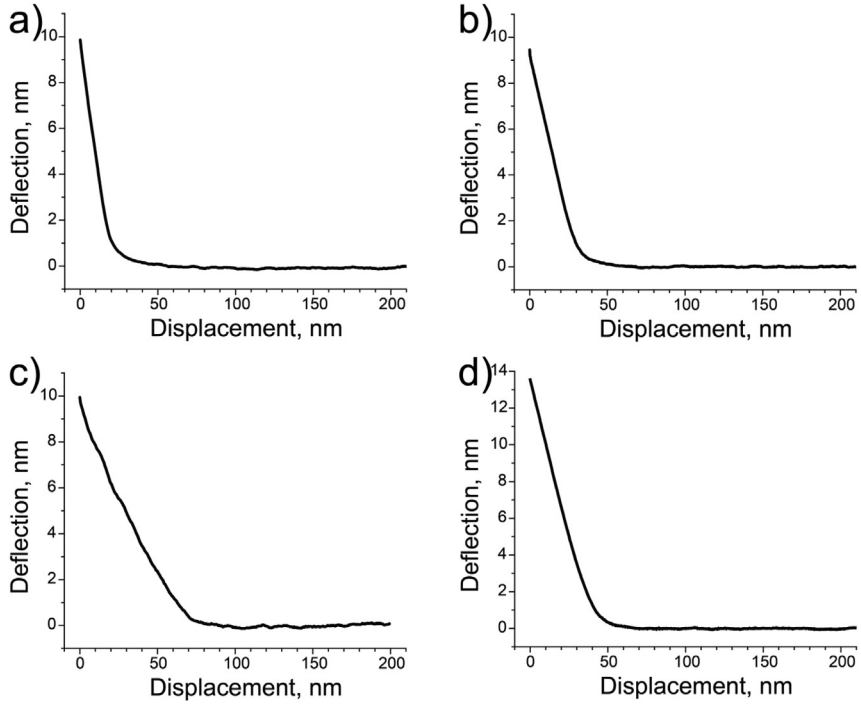

Fig. 3. Typical deflection curves for indentation experiments with ~10 nm setpoint performed on the surface of: a) Lotrafilcon B, b) Balafilcon A, c) Senofilcon A, d) Comfilcon A.

Resulting calculated moduli are 0.45 ± 0.07 MPa and 3.69 ± 0.36 MPa for the first layer and second layer, respectively. For Balafilcon A lenses, the thickness of the coating is lower, on the order of 15 nm and both first and second layer moduli are lower (0.21 ± 0.06 MPA and 1.35 ± 0.12 MPa respectively).

Fig. 3c shows a typical indentation curve for the surface of the Senofilcon A lens. Senofilcon A belongs to the second generation of lens materials, where hydrophilic properties were introduced through the internal wetting agent, poly(vinyl pirrolidone) (PVP) [7]. Therefore this material does not have to be treated to provide wettability to the surface. $\delta^{3/2}$ vs force data (Fig. 4c) exhibits constant slope through the indentation experiment with calculated modulus of 1.49 ± 0.28 MPa.

Finally, Comfilcon A represents the third generation of silicone-hydrogel materials, which contains hydrophilic chain segments within its structure and therefore it is inherently wettable [52]. From penetration versus force data one can observe slope variation with increased indentation depth (Fig. 3d). However, unlike the case of Lotrafilcon B and Balafilcon A lenses, the initial region does not have a linear part; the slope of the penetration data starts to decrease immediately after the contact point. Eventually the slope reaches constant value, which corresponds to 1.59 ± 0.17 MPa elastic modulus at deeper penetrations.

It is important to note, that all indentations performed in this study were nondestructive to the lens surfaces. Low forces were applied to the cantilever to avoid irreversible changes of the lens surface. Imaging of the surface of the lens after the indentation experiments showed no indentation marks. In addition linear penetration vs. force plots suggest pure elastic deformations, which further supports the purely elastic deformation and full surface recovery under given indentation conditions.

3.3. Lens cross sections

In surface mapping, the probing depth of the SFS indentation experiments is negligible as compared to the thickness of the lens. Maximum penetration depth reached in the present study is 100 nm, while thickness of the lens is in the 50–100 μm range [11]. Therefore, to study the mechanical properties of the sub-surface and bulk regions of the lens material it is necessary to make a cross section of the lens and perform indentations within the bulk of the lens. The QNM images were used as a contrast map to locate regions with different mechanical properties. Next, indentation experiments were performed in these regions, with the same fitting procedure discussed in the surface analysis section. Despite the fact that fast rate QNM scans show the presence of adhesive forces on the lens materials, all indentation curves collected during SFS scans showed no adhesion. Cross-sectional profiles were taken from each of the channels going across regions with property variation. Unlike the indentation curves taken from the surface of

Table 3
Summary of elastic moduli calculated from indentation experiments on the lens surface, lens cross sections and literature values of manufacturer reported elastic modulus from.[53].

Material	Surface indentations, MPa		Cross section indentations, MPa		Manufacturer reported, bulk, MPa
	First layer	Second layer	Outer layer	Bulk	
Lotrafilcon B	0.45 ± 0.07	3.69 ± 0.36	2.92 ± 0.52	2.77 ± 0.15	1.0
Balafilcon A	0.21 ± 0.06	1.35 ± 0.12	N/A[a]	3.11 ± 0.43[a]	1.1
Senofilcon A	0.52 ± 0.07	N/A	0.66 ± 0.18/4.38 ± 0.78	1.49 ± 0.28	0.72
Comfilcon A	1.59 ± 0.17	N/A	1.59 ± 0.26	1.75 ± 0.26	0.75

[a] Both bulk and outer layer of Balafilcon A contain inclusions with modulus of 1.74 ± 0.29 MPa.

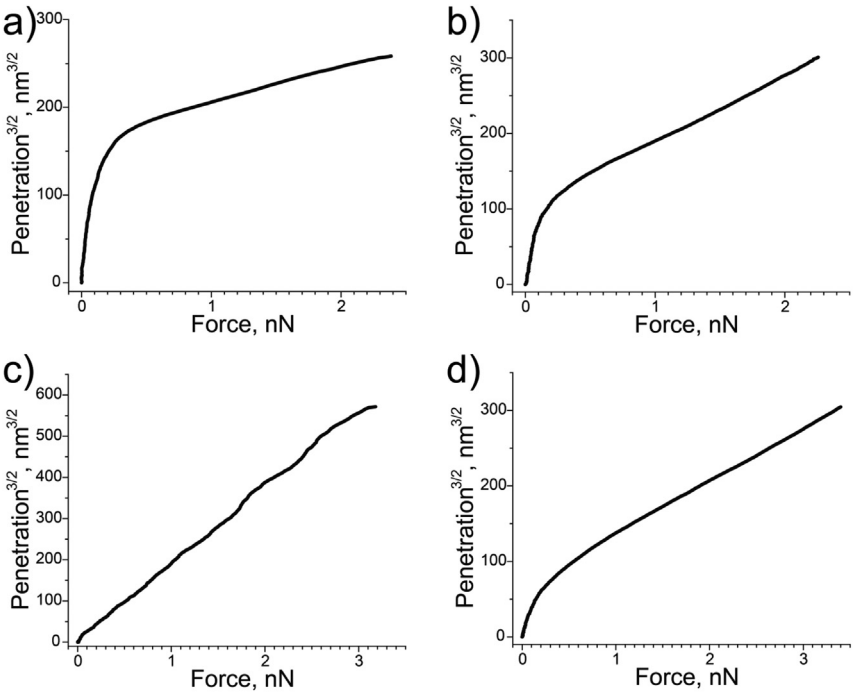

Fig. 4. Typical $\delta^{3/2}$ vs force plots derived from FDCs shown in Fig. 3: a) Lotrafilcon B, b) Balafilcon A, c) Senofilcon A, d) Comfilcon A.

Lotrafilicon A and Balafilcon A, all indentation curves acquired from the cross section displayed constant elastic modulus for each indentation depth. Results of these measurements are summarized in Table 3. Detailed results of the cross section measurements for all lens materials under fluid are presented below.

3.3.1. *Lotrafilcon B*

The results of QNM imaging of Lotrafilcon B lens are presented In Fig. 5. The edge of the cross section is located on the left side. Each of the channels shows two distinct regions: the bulk of the lens and an approximately 14 μm thick outer layer. The outer layer

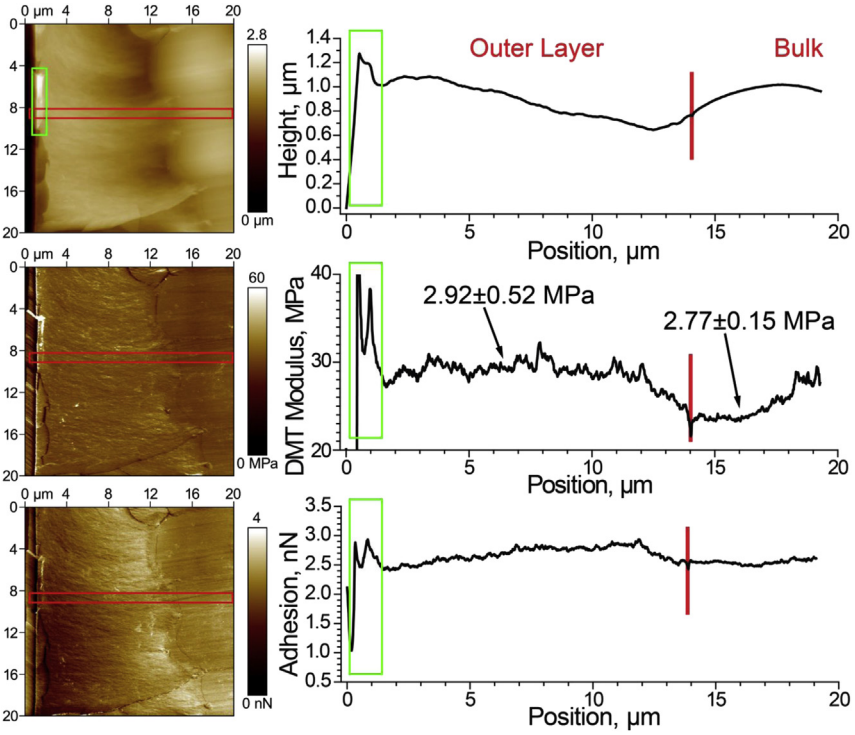

Fig. 5. QNM mapping of Lotrafilcon B section in topography, DMT modulus and adhesion channels. The red rectangle shows position of the profile section. The green rectangle shows the outer coating position. (For interpretation of the references to color in this figure legend, the reader is referred to the web version of this article.)

appears to be swollen and has an increased height as compared to the bulk of the lens. The portion of the outer layer which is closest to the edge bears a resemblance to an additional coating of ~200 nm thick (green rectangle outline, Fig. 5). This coating however is mostly torn away by the razor blade during lens cutting procedure.

FV measurements of the bulk of the lens and the outer layer show elastic modulus of 2.77 ± 0.15 MPa and 2.92 ± 0.52 MPa respectively. The additional outer coating was too thin and tilted to perform quantitative FV measurements on, however the DMT modulus channel of QNM measurements show slightly increased modulus for this coating (green rectangle outline, Fig. 5). This result is consistent with the surface measurements, where the modulus in this region was found to be 3.69 ± 0.36 MPa. Due to the low thickness and the edge effects, the 25 nm thick plasma coating cannot be imaged reliably from the cross section measurements.

3.3.2. Balafilcon A

Fig. 6 shows the surface of the cross section of Balafilcon A lens material. All channels show two distinct regions. The bulk of the lens is flat and smooth and the outer region is ~10 μm thick and contains some lamellar morphology.

Elastic modulus mapping of both the outer coating region and the bulk yielded similar values, with the elastic modulus of the bulk found to be 3.11 ± 0.41 MPa. Quantitative measurements of the modulus near the edge of the lens cross section could not be performed due to the high roughness of the sections at that location. Both regions have elongated inclusions with lower modulus (1.74 ± 0.29 MPa) material distributed within them. Since the measured modulus depends strongly on the topography of the surface at the point where the indentation is performed [13], care should be taken in assigning the value to the selected features.

Fig. 7 shows 1 μm^2 offline zoom in of one of these elongated inclusions (green box in Fig. 6B). One can clearly see, that the AFM tip can reach the bottom of the inclusion, which is 40–50 nm deep and 200 nm wide.

This height variation in the lens cross section was likely caused by cutting due to the mechanical properties difference between bulk of the lens and the inclusions. Since the bottom of the inclusion is relatively flat and its width is much bigger than the radius of curvature of the tip (see Fig. 1c), one can reliably perform indentation experiments to calculate the modulus of the inclusion in the wet state. It is interesting to note that SEM studies of the same material performed in vacuum showed porous structure instead of compliant inclusions imaged here by AFM under wet conditions [54].

3.3.3. Senofilcon A

The Senofilcon A lens shows a distinct boundary between the bulk of the lens and the outer layer of ~4 μm thickness in all three channels (Fig. 8). The outer layer has higher roughness and lower modulus and adhesion than the bulk of the lens. Calculated modulus was found to be 1.49 ± 0.28 MPa for the bulk and 0.66 ± 0.18 MPa for the outer layer (Table 3). The modulus for the outer layer is close to the modulus calculated from the surface indentation (0.52 ± 0.07 MPa). The case of Senofilcon A lenses demonstrates that in order to study the stiffness of soft contact lenses using SFS with a sharp tip, surface indentations alone are insufficient.

In this study, we observed that the outer layer of Senofilcon A has multiple inclusions of higher modulus (Figs. 8 and 9). From the adhesion mapping one can clearly see the effect of topography on the measurements: the adhesion has a spike on the right side of the inclusion, suggesting higher area of contact between the tip and the material when, in addition to the tip apex, the side of the tip comes into the contact with the material. Nevertheless there are flat regions within the inclusions, where the accurate measurements could be performed. The resulting modulus for the inclusions was calculated to be 4.38 ± 0.78 MPa. This value has high standard deviation due to the topographical irregularities of the inclusions.

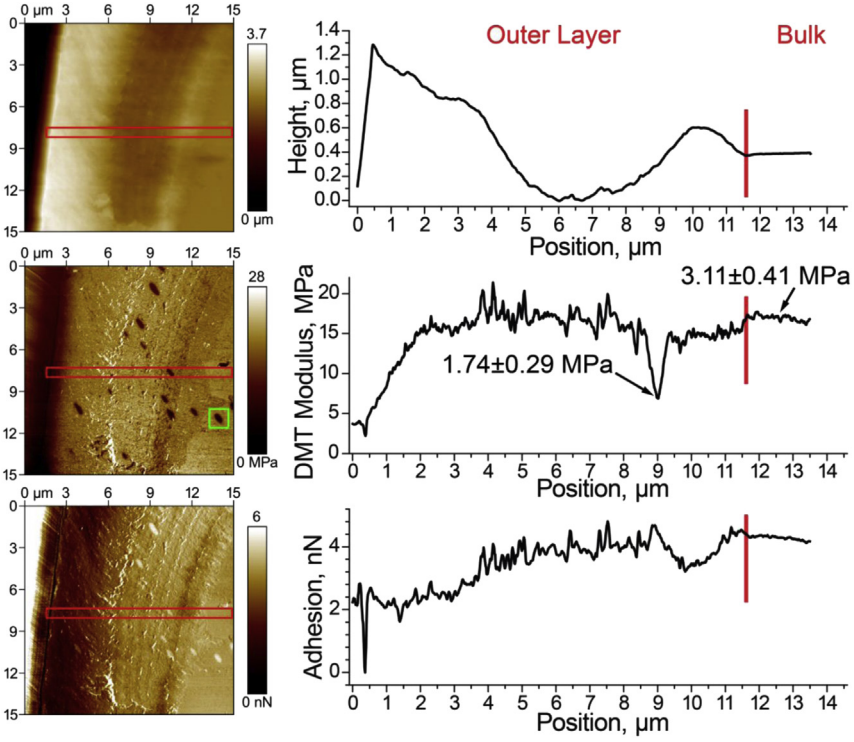

Fig. 6. QNM mapping of Balafilcon A section in topography, DMT modulus and adhesion channels. The red rectangle shows position of the profile section. The green square shows the position of zoom in shown in Fig. 7. (For interpretation of the references to color in this figure legend, the reader is referred to the web version of this article.)

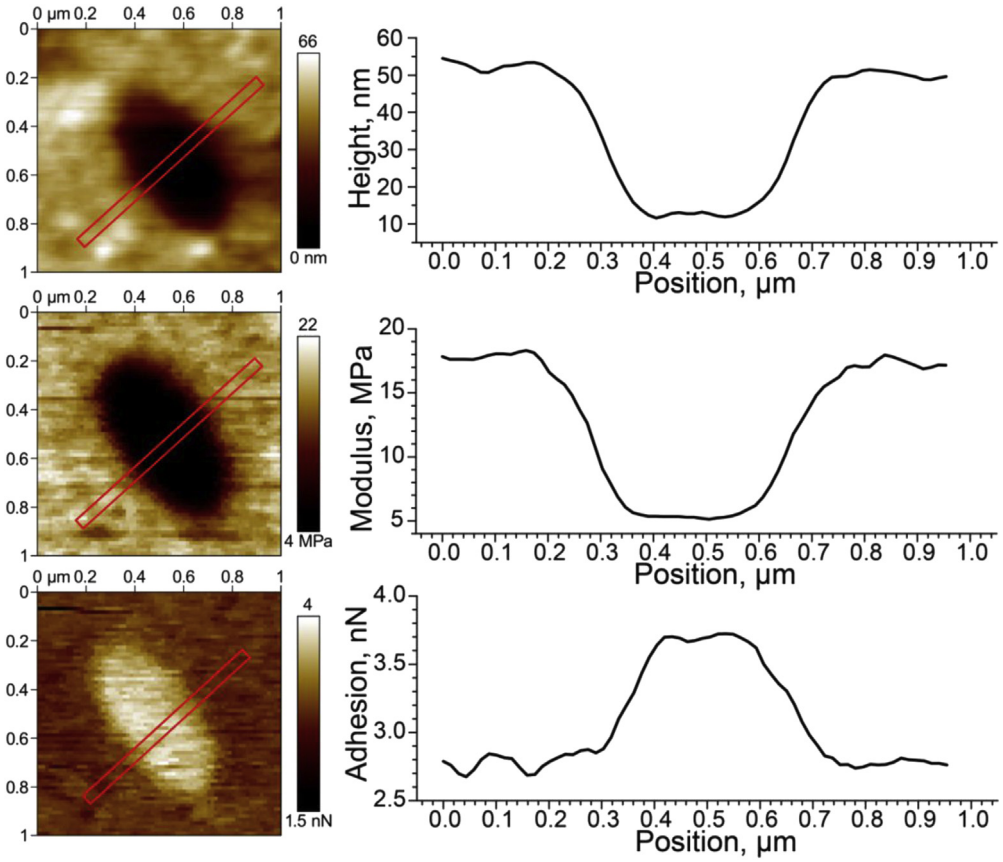

Fig. 7. QNM mapping of Balafilcon A section in topography, DMT modulus and adhesion channels (zoom in from Fig. 6). The red rectangle shows the profile section. (For interpretation of the references to color in this figure legend, the reader is referred to the web version of this article.)

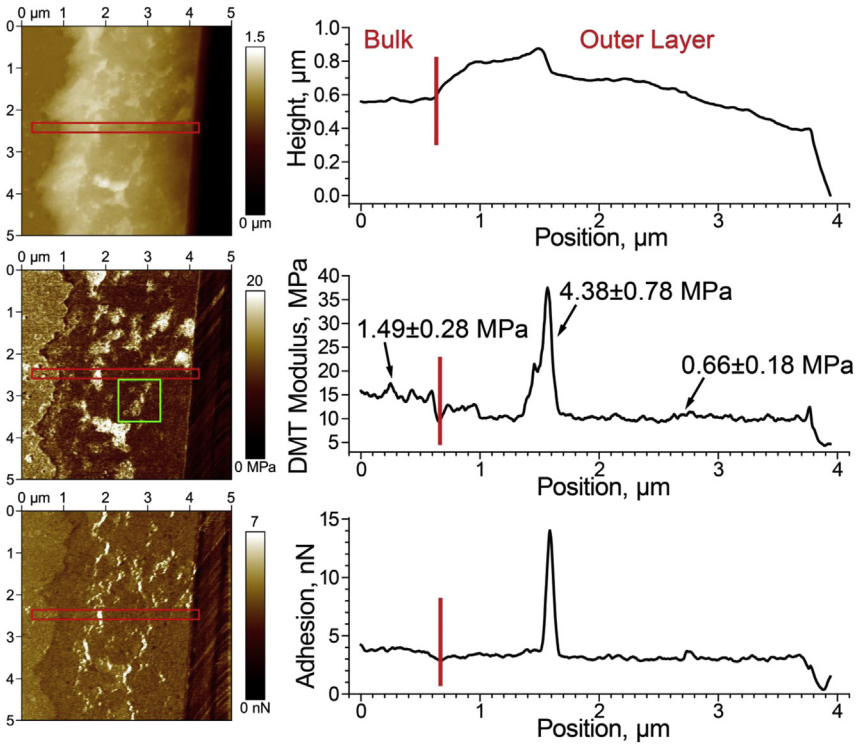

Fig. 8. QNM mapping of Senofilcon A section in topography, DMT modulus and adhesion channels. Red rectangle shows position of the profile section. The green square shows the position of zoom in, shown in Fig. 9. (For interpretation of the references to color in this figure legend, the reader is referred to the web version of this article.)

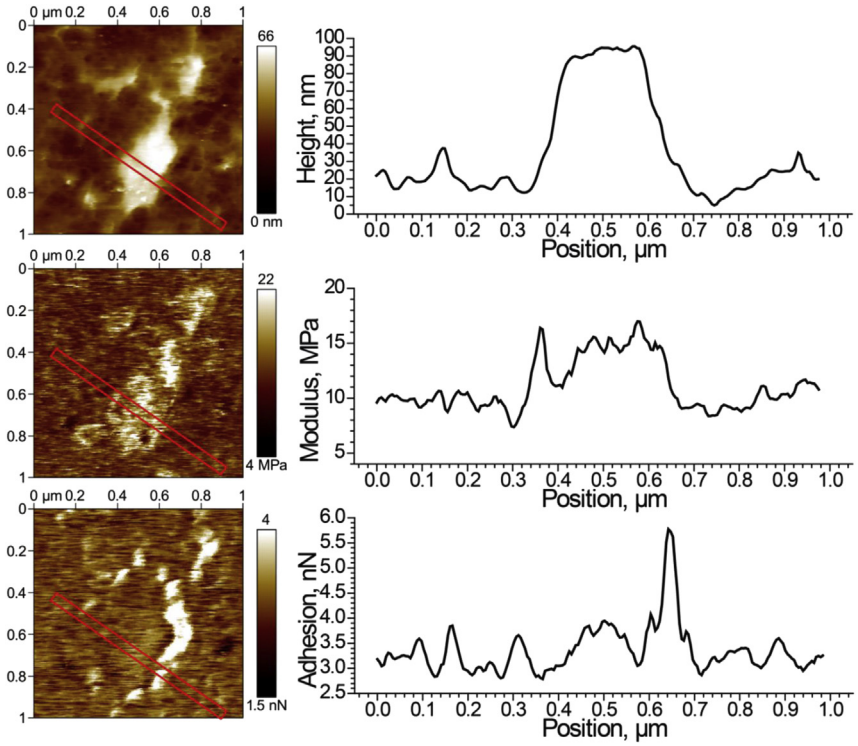

Fig. 9. QNM mapping of Senofilcon A section in topography, DMT modulus and adhesion channels, zoom in from Fig. 8. The red rectangle shows position of the profile section. (For interpretation of the references to color in this figure legend, the reader is referred to the web version of this article.)

3.3.4. *Comfilcon A*

The Comfilcon A lens section shows ~5 μm coating with modulus of 1.59 ± 0.26 MPa, which is slightly lower than the modulus of the bulk, 1.75 ± 0.26 MPa (Fig. 10). The outer layer appears to be swollen as compared to the bulk. Irregularities in the modulus and adhesion mappings are caused by fluctuations in the topography. However, for modulus measurements the flattest surface regions were selected. As with the Senofilcon A lens, the modulus of the coating closely matches the modulus measured with surface indentation. However, since the thickest portion of the

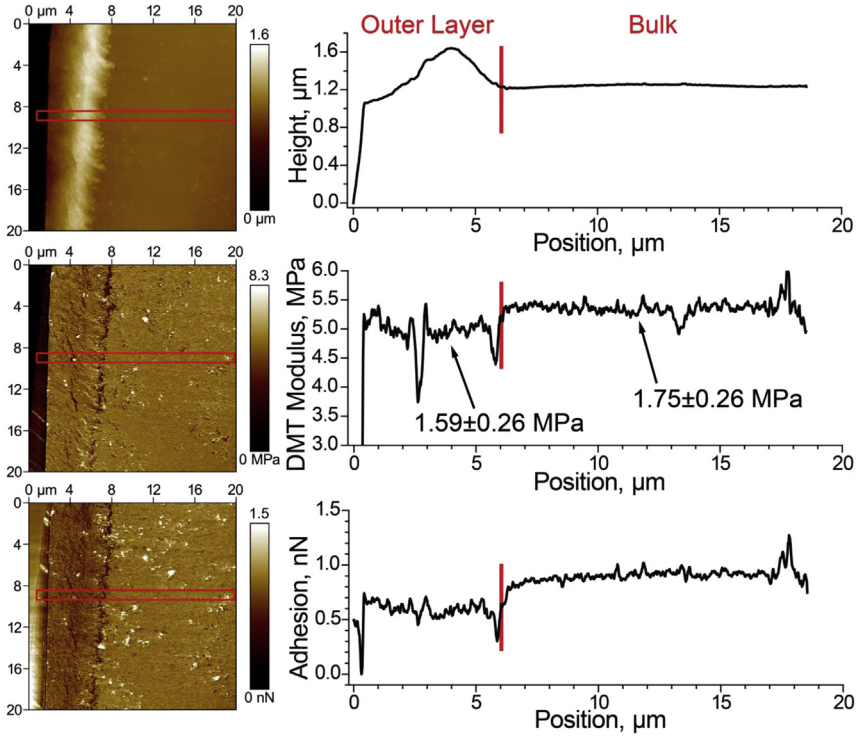

Fig. 10. Peakforece QNM characterization of Comfilcon A section in topography, DMT modulus and adhesion channels. The red rectangle shows position of the profile section. (For interpretation of the references to color in this figure legend, the reader is referred to the web version of this article.)

lens can reach ~100 μm, the bulk portion will mostly contribute to the structural modulus of the whole lens.

3.4. Comparative analysis of measured moduli

Table 3 shows accumulative data for the measured bulk modulus of all four studied materials along with the values reported in the literature. It is worth noting that for all the lens materials the elastic modulus from SFS measurements is consistently 2–2.5 times higher than the value reported by the manufacturer. For Balafilcon A lenses, the trend is different, with measured values being ~3 times higher. However, since lens manufacturers employ conventional tensile testing [11], the presence of compliant inclusions would lower the overall modulus of the material (Fig. 6).

Additionally, we can associate the above-mentioned difference in modulus values with viscoelastic effects in the measured materials. These effects are known to manifest themselves in the rate dependence of elastic properties in soft polymer materials in the swollen state and in the vicinity of glass transition [42]. In the work of Horst et al. [11], where the values of elastic modulus were found to be similar to the ones reported by manufacturers for Balafilcon A and Senofilcon A (1.1 MPa and 0.7 MPa respectively), a strain rate of 1% per second was used.

For the AFM indentation experiments the strain induced within the material can be estimated as $\varepsilon = a/R$, where a is the radius of contact between the surface and the indenter, and R is the radius of curvature of the indenter [55]. Since under Sneddon's assumptions for parabolic indenter $a = \delta R$ [41], one can estimate strain for low indentation depths as:

$$\varepsilon = \sqrt{\delta/R} \tag{2}$$

From Eq. (1) it follows that at the constant loading rate penetration δ changes nonlinearly with time, however here for the comparative study we will estimate the strain rate as strain at maximum penetration divided by the time of indentation experiment.

Taking the indentation into the bulk of Lotrafilcon B as an example such estimation results in extremely high strain rate of 6200% per second for 4 Hz experiment frequency (this frequency was used in FDC measurements in this study). According to the general theory of polymer elasticity, a material becomes stiffer at higher loading rates [56], therefore indentation measurements would produce higher values of the elastic moduli for the lens materials than the literature values of conventional tensile measurements. To prove this concept, frequency dependent measurements were performed on the bulk region of Lotrafilcon B lens as an example. In addition, similar measurements were performed on a purely elastic PDMS sample with the well-known elastic properties. Due to the nonlinearity in the penetration rate, a single constant value of strain rate cannot be assigned to each indentation experiment. Therefore here we will use indentation time (period when tip and the sample are in contact during the approach portion of the indentation cycle) as a variable to show changes in elastic modulus (Fig. 11).

The standard measurements performed in this work for Lotrafilcon B lens at the 4 Hz frequency corresponds to an indentation time of 0.07 s and the apparent modulus value decreases with the increase in the indentation time as expected for viscoelastic materials. The values exhibit linear decrease with time when plotted in logarithmic scale, which suggests well known Williams-Landel-Ferry (WLF) dependence, common for polymer materials [57]. Calculated virtual indentation time, which corresponds to the 1% strain rate of conventional tensile measurements, is indicated by 'X' mark in Fig. 11a. The literature value of the modulus at this point for

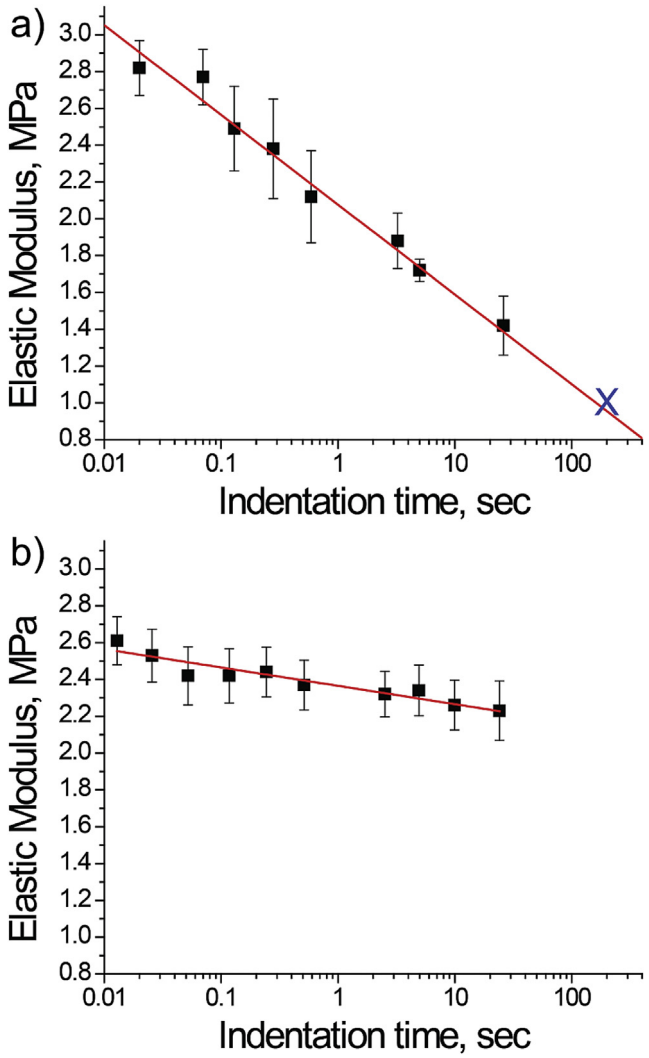

Fig. 11. Elastic modulus values vs indentation time for: a) bulk cross section of Lotrafilcon B and b) PDMS sample. Lines show linear fit in logarithmic scale. X mark shows approximate time of indentation, which corresponds to 1% per second strain rate.

Lotrafilcon B lens is 1 MPa, and as one can see the fitting line for the experimental data tends close to this value. However reliable AFM measurements with such long indentation times cannot be reliably performed due to piezo-creep effects. In contrast, similar indentation experiments for PDMS samples (Fig. 11b) show very little variation with indentation time and elastic modulus values close to literature [58].

4. Conclusions

Experimental protocol for measurements of the soft composite polymeric materials is suggested here with soft silicone hydrogel contact lens materials used as an example. Results from the high resolution QNM mode combined with standard SFS measurements of the surfaces and cross sections of four commercially available contact lenses are presented. Measurements of the surface topography of the lenses revealed smooth areas suitable for indentation measurements. Surface indentations curves exhibited Sneddon's model behavior, which allowed for the calculation of elastic modulus. Additionally, surface indentation experiments on Lotrafilcon B and Balafilcon A materials revealed the presence of a thin coating resulting from plasma treatment of these lenses during

their fabrication. Cross sectional measurements of the lens materials showed the capability of the SFS to resolve surface features with high special resolution and revealed the presence of the composite subsurface regions with variations of adhesive and mechanical properties within the interior of the lens. SFS measurements were used to acquire precise quantitative mechanical properties for these regions in order to provide a full picture of mechanical behavior.

Values of the measured elastic moduli for the bulk portion of the studied lens materials were found to be higher than those reported in literature, however when examined in relation to each other a similar trend was observed. Additionally, the discrepancy between the measurements presented here and those previously reported in literature can be attributed to the differences in the strain rate between Instron and indentation measurements. Frequency variation experiments with Lotrafilcon B sample showed the elastic modulus variation with frequency, with the modulus value for Lotrafilcon B tending to the literature value for measurement rates close to the literature data. The experimental values acquired for all lens materials at 4 Hz present physically relevant quantities, which can be used for the lens comparison and the proposed method can be employed for comparable measurements of mechanical properties of soft contact lenses under practical conditions.

Acknowledgments

Financial support from National Science Foundation, Division of Materials Research under World Materials Network Award DMR-1209332 and DMR-1002810 as well as Microanalysis Center, Georgia Institute of Technology. We thank Anna Hoffman for the help with calculations.

Appendix A. Supplementary data

Supplementary data related to this article can be found at http://dx.doi.org/10.1016/j.polymer.2014.09.053.

References

[1] Efron N. Aust J Optom 1980;63:273–9.
[2] Sorbara L, Jones L, Williams-Lyn D. Cont Lens Anterior Eye 2009;32:93–6.
[3] González-Méijome JM, González-Pérez J, Cerviño A, Yebra-Pimentel E, Parafita MA. Optom Vis Sci 2003;80:440–6.
[4] Nicolson PC, Vogt J. Biomaterials 2001;22:3273–83.
[5] French K. Optician 2005;230:29–34.
[6] Stapleton F, Stretton S, Papas E, Skotnitsky C, Sweeney DF. Ocul Surf 2006;4:24–43.
[7] French K, Jones L. Optom Today 2008;48:38–43.
[8] Szczotka-Flynn L. Optom Manag 2008;43:68–71.
[9] Tranoudis I, Efron N. Cont Lens Anterior Eye 2004;27:177–91.
[10] Young G, Garofalo R, Harmer O, Peters S. Cont Lens Anterior Eye 2010;33:210–4.
[11] Horst CR, Brodland B, Jones LW, Brodland GW. Optom Vis Sci 2012;89:1468–76.
[12] Weikart CM, Matsuzawa Y, Winterton L, Yasuda HK. J Biomed Mater Res 2001;54:597–607.
[13] Tsukruk VV, Singamaneni S. Scanning probe microscopy of soft matter: fundamentals and practices. Wiley-VCH Verlag GmbH & Co. KGaA; 2011.
[14] McConney ME, Singamaneni S, Tsukruk VV. Polym Rev 2010;50:235–86.
[15] Lisunova MO, Drachuk I, Shchepelina OA, Anderson KD, Tsukruk VV. Langmuir 2011;27:11157–65.
[16] Young SL, Chyasnavichyus M, Erko M, Barth FG, Fratzl P, Zlotnikov I, et al. Acta Biomater 2014;10:4832–42.
[17] Last JA, Russell P, Nealey PF, Murphy CJ. Invest Ophthalmol Vis Sci 2010;51:6083–94.
[18] Chizhik S, Huang Z, Gorbunov VV, Myshkin N, Tsukruk VV. Langmuir 1998;14:2606–9.
[19] Tsukruk VV, Huang Z, Chizhik S, Gorbunov VVS. J Mat Sci 1998;33:4905–9.
[20] Tsukruk VV, Huang Z. Polymer 2000;41:5541–5.
[21] Tsukruk VV, Gorbunov VV, Huang Z, Chizhik SA. Polym Intern 2000;49:441–4.
[22] Tsukruk VV, Sidorenko A, Yang H. Polymer 2002;43:1695–9.
[23] Lemieux M, Minko S, Usov D, Stamm M, Tsukruk VV. Langmuir 2003;19:6126–34.
[24] Lemieux M, Usov D, Minko S, Stamm M, Shulha H, Tsukruk VV. Macromolecules 2003;36:7244–55.
[25] Shulha H, Po Foo CW, Kaplan DL, Tsukruk VV. Polymer 2006;47:5821–30.
[26] Picart C, Senger B, Sengupta K, Dubreuil F, Fery A. Colloid Surf A 2007;303:30–6.
[27] Cicoira F, Samorì P. STM and AFM studies on (bio) molecular systems: unravelling the nanoworld. Springer; 2008.
[28] Guryča V, Hobzová R, Přádný M, Sirc J, Michálek J. Cont Lens Anterior Eye 2007;30:215–22.
[29] Kim SH, Marmo C, Somorjai GA. Biomaterials 2001;22:3285–94.
[30] Teichroeb JH, Forrest JA, Ngai V, Martin JW, Jones L, Medley J. Optom Vis Sci 2008;85:1151–64.
[31] Anderson MS, Gaimari SD. J Struct Biol 2003;142:364–8.
[32] Opdahl A, Kim SH, Koffas TS, Marmo C, Somorjai GA. J Biomed Mater Res A 2003;67:350–6.
[33] Kim SH, Opdahl A, Marmo C, Somorjai GA. Biomaterials 2002;23:1657–66.
[34] Yablon DG. Scanning probe microscopy for industrial applications: nanomechanical characterization. Wiley; 2013.
[35] Butt H-J, Cappella B, Kappl M. Surf Sci Rep 2005;59:1–152.
[36] Johnson KL. Contact mechanics. Cambridge university press; 1987.
[37] Young SL, Gupta M, Hanske C, Fery A, Scheibel T, Tsukruk VV. Biomacromolecules 2012;13:3189–99.
[38] van der Werf KO, Putman CAJ, de Grooth BG, Greve J. Appl Phys Lett 1994;65:1195–7.
[39] Du P, Lu H, Zhang X. Mater Res Soc Symp Proc 2009;1222:1202–3.
[40] Tian F, Qian X, Villarrubia JS. Ultramicroscopy 2008;109:44–53.
[41] Adamcik J, Berquand A, Mezzenga R. Appl Phys Lett 2011;98:193701–3.
[42] Sneddon IN. Int J Eng Sci 1965;3:47–57.
[43] Chyasnavichyus M, Young SL, Tsukruk VV. Langmuir 2014;30:10566–82.
[44] Cappella B, Silbernagl D. Langmuir 2007;23:10779–87.
[45] Schneider A, Francius G, Obeid R, Schwinté P, Hemmerlé J, Frisch B, et al. Langmuir 2005;22:1193–200.
[46] Halperin A, Zhulina EB. Langmuir 2010;26:8933–40.
[47] González-Méijome JM, López-Alemany A, Almeida JB, Parafita MA, Refojo MF. J Biomed Mater Res B 2006;76B:412–8.
[48] González-Méijome JM, López-Alemany A, Almeida JB, Parafita MA. J Biomed Mater Res B 2009;88B:75–82.
[49] Giraldez M, Garcia-Resua C, Lira M, Sánchez-Sellero C, Yebra-Pimentel E. Proc SPIE 2011:80010–8.
[50] Kovalev A, Shulha H, Lemieux M, Myshkin N, Tsukruk V. J Mater Res 2004;19:716–28.
[51] Jones L, Subbaraman L, Rogers R, Dumbleton K. Optician 2006;232:28–34.
[52] Jones L. Cont Lens Spec 2007;22:15.
[53] French K, Jones L. Optom Today 2008;48:42–6.
[54] López-Alemany A, Compañ V, Refojo MF. J Biomed Res 2002;63:319–25.
[55] Tabor D. The hardness of solids. Rev Phys Technol 1970;1:145.
[56] Shulha H, Kovalev A, Myshkin N, Tsukruk VV. R Eur Polym J 2004;40:949–56.
[57] Williams ML, Landel RF, Ferry JD. J Am Chem Soc 1955;77:3701–7.
[58] Le Rouzic J, Delobelle P, Vairac P, Cretin B. Eur Phys J Appl Phys 2009;48:11201.